AUTOMATION OF PNEUMATIC THROTTLE CHECK VALVES BY USING NOVEL MULTI-STABLE SOLENOIDS

Thomas Kramer*, Jürgen Weber

Chair of Fluid-Mechatronic Systems (Fluidtronics), Institute of Mechatronic Engineering, Technische Universität Dresden, Helmholtzstrasse 7a, 01069 Dresden

* Corresponding author: Tel.: +49 351 463-31964; E-mail address: thomas.kramer@tu-dresden.de

ABSTRACT

Multi-stable solenoids are novel energy-efficient actuator structures, which can hold any armature position powerless. Power is only required to change the armature position. They combine the continuous adjustability of proportional solenoids with the energy efficiency of polarised magnetic circuits. Thus, they are well suited for automating pneumatic throttle check valves, in order to set the throttle cross section and thus the cylinder piston velocity to a specific value and hold it for a certain time. This is useful in industry 4.0 context to produce on demand with various required piston velocities or for gradual compensation for increasing frictional forces during cylinder lifetime.
The focus of this paper is the application of novel multi-stable solenoids for replacing the todays widely used manual adjustment of throttle check valves. Therefore, two different throttle valves are designed: a spool valve and a poppet valve. They are based on the transfer characteristic of a conventional throttle check valve. The flow behaviour of both valves is investigated to show the principal transfer behaviour and disturbances. The valves are equipped with a multi-stable solenoid for demonstrating the adjustability of the throttle's volume flow rate and on that basis the adjustability of the piston velocity in a pneumatic cylinder drive.

Keywords: multi-stable solenoid, solenoid, pneumatic, throttle check valve, automation

1. INTRODUCTION

Electro-mechanical transducers are key components of fluid power systems. Especially as valve drives, solenoids based on the reluctance principle are widely used. For such solenoids, various design and operating principles have been established [1]. These can be arranged concerning the output behaviour (switching, continuous) and the magnetic circuit design (neutral, polarised) according to **Table 1**. Stable states are defined by no current flowing.

Table 1: Classification of existing solenoid principles

	switching (limited position number)	**continuous** (proportional)
neutral magnetic circuit	mono-stable switching solenoid	mono-stable proportional solenoid
polarised magnetic circuit	bi-stable, tri-stable, … switching solenoid	

Neutral magnetic circuits as mono-stable solenoids with their simple design are widely used. They consist of a coil, a yoke as fixed soft magnetic part and a movable soft magnetic armature, as seen in **Figure 1** left. The coil generates a magnetic field in the magnetic parts depending on the coil current i. The resulting magnetic flux Φ leads to a magnetic force F_m, which acts on the armature. In combination with a spring, an armature position x_a can be set according to the force balance of spring force F_s and magnetic force F_m. Such solenoids require a continuous power supply to hold any position except for the stable one given by the spring force (maximum air gap $x_\mathrm{a,max}$).

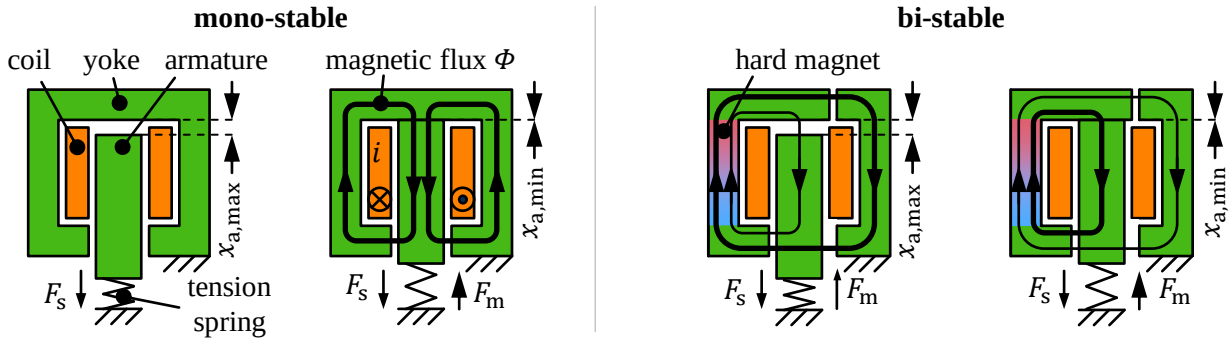

Figure 1: Principal design of neutral mono-stable and polarised bi-stable switching solenoid (based on [2])

Bistable solenoids [3–5] or solutions with more than two, but a limited number of stable switching positions [6, 7], are an efficient alternative to neutral mono-stable switching solenoids. Therefore, different design principles are known [2, 3]. Additional to the soft magnetic parts, they consist usually of a hard magnetic part, as seen in **Figure 1** right. This leads to a magnetic flux even without exciting the coil. The magnetic circuit is polarised. Thus, two holding forces can be realised, which can be hold without power supply: a spring force and a permanent magnetic force. The two holding forces result in two stable armature positions $x_{a,min}$ and $x_{a,max}$. The switching between the positions is realised only by a short current pulse through the integrated coil. The existing solutions of polarised magnetic circuits aim only at a limited number of switching positions.

Multi-stable solenoids

In order to combine both, the energy efficiency and the continuous adjustability, multi-stable solenoids are currently a focus of research. In [8], an approach for such multi-stable solenoids is published. The working principle utilises the inner magnetic hysteresis behaviour of semi-hard magnetic material. Such materials have a high energy storage capability and can be polarised by the solenoid's integrated coil. **Figure 2** illustrates the working principle with the material behaviour $B(H)$ and the basic design of multi-stable solenoids.

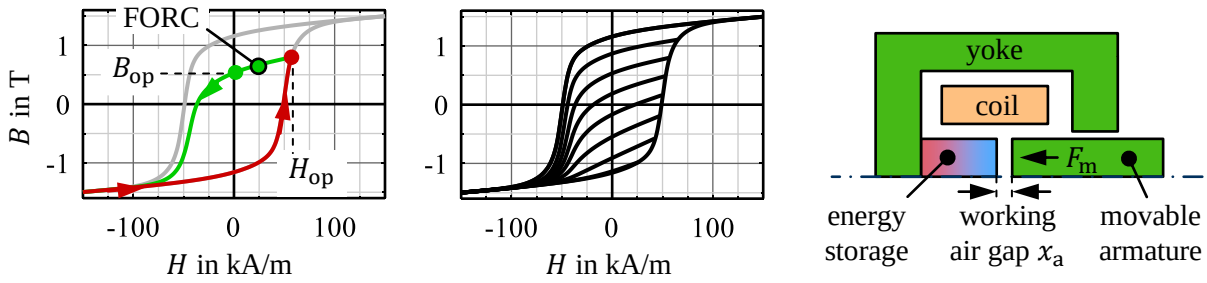

Figure 2: Magnetisation procedure for FORC generation (left), set of FORCs (middle), both for anisotropic CROVAC 12 from measurements using a self-made hysteresisgraph for hard magnetic materials (principle according to [9]), principal design of multi-stable solenoids (right)

The inner magnetic hysteresis behaviour can be accesses by so-called first order reversal curves (FORC). Therefore, the material is first magnetised along an outer hysteresis branch starting at saturation as reference (red line). After field reversal at any operating point H_{op}, the associated FORC arises (green line). If the external field H is shut down, the remanent magnetic flux density B_{op} remains. Depending on the reversal point H_{op}, any remanent point in the hysteresis loop can be reached as shown in **Figure 2** middle. Thus, the semi-hard magnetic material acts as variable magnetic energy storage.

The design of the proposed multi-stable solenoids is as simple as possible. The magnetic circuit consists of the energy storage, a yoke and an armature. The coil is in the center. With a pulsed coil excitation, a magnetic field is generated mostly in the energy storage for polarising it to a certain level. After shutting off the pulse, the remanent operating point according to the $B(H)$-behaviour is set. This leads to the proposed actuator functionality, where any operating point can be set and hold without additional power supply.

For detailed designing, an analytical approach was developed. The inputs of the approach are the maximum force potential $F_{\mathrm{m,max}}$ at a given air gap width $x_{\mathrm{a,max}}$, a semi-hard magnetic material behaviour, an air gap design and power supply parameters. Outputs are the size of the energy storage and the coil parameters. On that basis, demonstrators with three different semi-hard magnetic materials were build up. The behaviour of the corresponding materials is shown in **Figure 3** left. The demonstrators with anisotropic CROVAC 12 and AlNiCo 9 are designed for $F_{\mathrm{m}} = 50$ N at $x = 2$ mm. The demonstrator for hard ferrite Y35 has a lower force potential $F_{\mathrm{m}} = 15$ N at $x = 2$ mm due to significant reduced remanent flux density B_{r}. **Figure 3** middle shows the maximum magnetic force of the demonstrators.

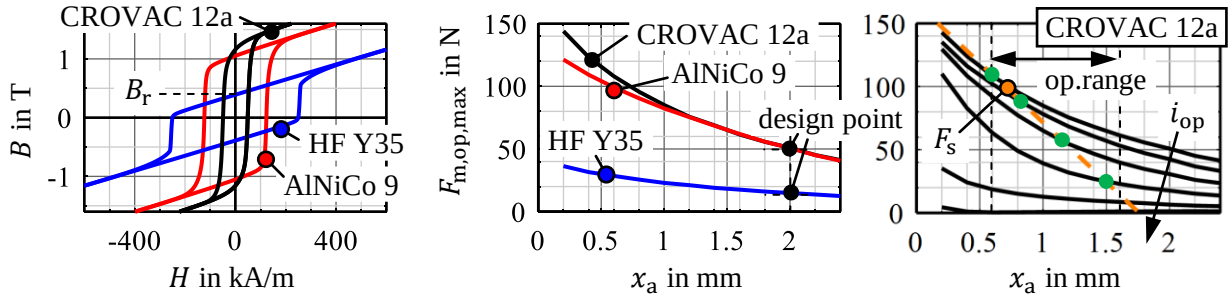

Figure 3: Magnetic material behaviour $B(H)$ of used energy storage materials (left), measured output behaviour $F_{\mathrm{m}}(x_{\mathrm{a}}, i_{\mathrm{op,max}})$ of the designed demonstrators at full polarisation (right), measured output behaviour $F_{\mathrm{m}}(x_{\mathrm{a}}, i_{\mathrm{op}})$ for setting remanent armature position at force balance points

For setting a remanent armature position, the magnetic force F_{m} has to act against a spring with the force F_{s}. Depending on the polarisation current i_{op}, any position can be set and held without power according to the force balance

$$F_{\mathrm{m,op}} = F_{\mathrm{s}} + F_{\mathrm{l}} = F_{\mathrm{s0}} - c x_{\mathrm{a,op}} + F_{\mathrm{l}}. \tag{1}$$

Therefore, **Figure 3** right shows the magnetic force characteristic for selected polarisation currents i_{op} and the resulting balanced operating points in green (see also [8]). Due to nonlinear force behaviour, the operating range is set by the spring to approximately 1 mm. It has to be taken into account that additional load forces F_{l} influence the force balance and thus the resulting armature position $x_{\mathrm{a,op}}$.

Applications of multi-stable solenoids

The potential fields of application for such novel multi-stable structures are manifold [8].

Especially in fluid power, new flexible and energy-efficient possibilities open up with this novel actuator principle. The manual adjustment of throttle check valves can be replaced, in order to adjust their opening cross-section automated during operation. This allows, for example, cylinder velocities to be set as required (industry 4.0: produce on demand) or a gradual compensation for increasing frictional forces during cylinder lifetime as a result of increasing seal wear. In addition, pressure relief, pressure reducing and proportional valves can be equipped with this novel actuator principle

to maintain any armature force or armature position without power.

In this paper, the focus is on automating pneumatic throttle check valves for demonstrating the novel actuator type in a real application. For this purpose, two throttles in form of a spool and a poppet valve are designed. The transfer characteristics of the throttles are measured to analyse the adjustability of the flow rate and to identify disturbance forces. The throttles are equipped with a suitable multi-stable solenoid demonstrator for investigating the setting of the throttle opening area and the resulting flow rate. The automated throttles are attached to a cylinder drive as meter-out flow control to demonstrate the setting of different cylinder piston velocities.

2. REFERENCE THROTTLE

Pneumatic cylinder drives are often equipped with a meter-out throttling to adjust the cylinder velocity $\dot{y}$ nearly independent from an external load force and from the supply pressure p_s as well as to increase the stiffness of the mechanical system. **Figure 4** left shows a corresponding circuit.

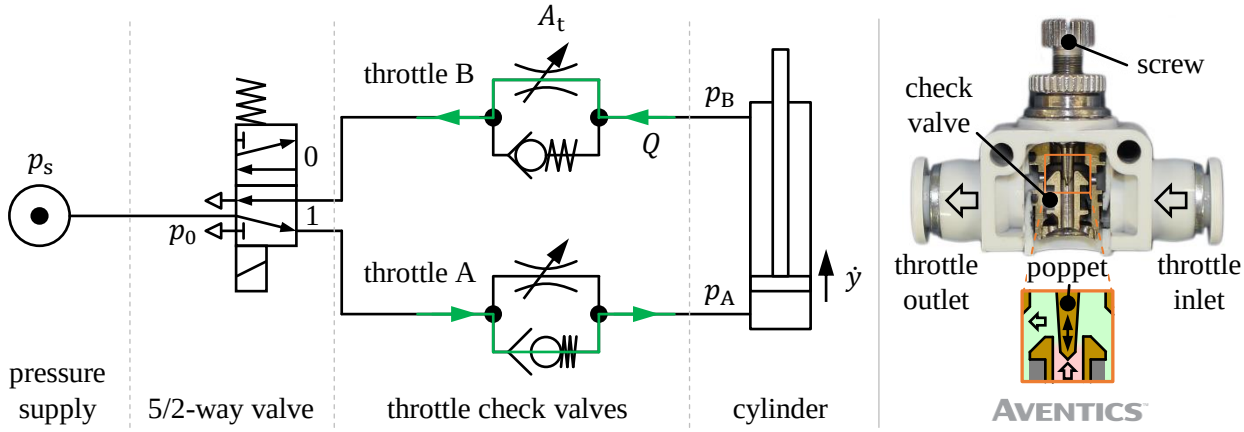

Figure 4: Pneumatic cylinder drive with meter-out control (left), reference throttle check valve as section model and principal cross section of throttle (right)

The metering is realized by two throttle check valves, one for each direction of movement. For moving the cylinder piston out, the mass flow goes through throttle B, as illustrated in the schematic. In contrast, throttle A flows through for moving in. By adjusting the throttle with the cross section A_t, the volume flow rate Q is set.

A common throttle for a typical cylinder size of 32 mm is an Aventics QR1-DBS-DA08, which is shown in **Figure 4** right. This throttle type is used in the paper as reference. The thumb screw serves for fine adjustment of the throttle cross section by moving the poppet. A key parameter of the throttle is the sonic conductance C at maximum opening. It is derived from measurements according to ISO 6358 [10], simplified for direct outlet to atmosphere with the pressure p_0. **Figure 5** left shows the measurement setup. It consists of a supply with variable pressure p_s, a volume flow rate sensor and a pressure sensor at the throttle inlet.

The supply pressure p_s is increased and decreased between 0 and 6 bar (relative) by manual adjustment of a usual pressure reducing valve. Meanwhile, relative inlet pressure p_1 and volume flow rate Q of the throttle are recorded. From the resulting $Q(p_1)$-behaviour in sonic range, the conductance is determined from the orange-coloured regression line with

$$C = \frac{\mathrm{d}Q}{\mathrm{d}p} = 39.4 \, \frac{\mathrm{Nl}}{\mathrm{min \cdot bar}} \tag{2}$$

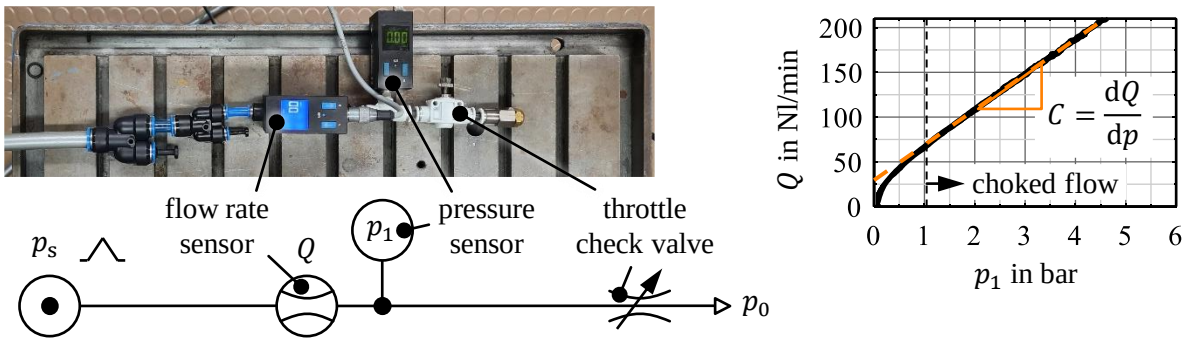

Figure 5: Measurement setup for characterising reference throttle Aventics QR1-DBS-DA08 (left), throttle transfer behaviour $Q(p_1)$ for determining sonic conductance (right)

3. THROTTLE DESIGN

On the base of the reference, two different throttles are designed and investigated: a spool valve and a poppet valve design. The spool valve is an ideal load case for the multi-stabile solenoid, since it has theoretically no relevant disturbing forces. The poppet valve is more a real load case for the multi-stable solenoid with its additional pressure force. Specific valves are necessary due to adaption to the multi-stable solenoid demonstrator.

For designing both throttle valves, the maximum cross section A_t has to be calculated from the reference sonic conductance. According to ISO 6358, the maximum mass flow rate is

$$\dot{m} = C p_1 \rho_0 \sqrt{\frac{T_0}{T_1}}, \tag{3}$$

considering a given pressure p_1 for choked flow and a given temperature T_1. In addition, the mass flow through a technical pneumatic resistance can be calculated by

$$\dot{m} = \alpha_\mathrm{d}\, A_\mathrm{t} \sqrt{2 p_1 \rho_1}\, \psi \tag{4}$$

[11]. The values are throttle parameters as cross section area A_t and discharge coefficient α_d, the air parameters pressure p_1 and density ρ_1 as well as the maximum value $\psi = 0.484$ of the discharge function considering choked flow.

By equating both, eq. (3) and (4), and using the ideal gas law, it results for the throttle cross section

$$A_\mathrm{t} = \frac{C p_0}{\alpha_\mathrm{d} \psi \sqrt{2 R_0 T_0}}. \tag{5}$$

The discharge coefficient α_d depends on the throttle design and is here assumed to a mid-size value $\alpha_\mathrm{d} = 0.7$ [11]. By applying eq. (5) with the sonic conductance from eq. (2), the maximum cross section of the reference throttle is $A_\mathrm{t,ref} = 4.7$ mm². This opening area serves as base for designing a comparable spool and poppet valve.

Spool design

For simple manufacturing, the throttle of the spool valve is realised by n_h cross holes with the diameter d_h. **Figure 6** left depicts the resulting throttle area exemplary at one hole.

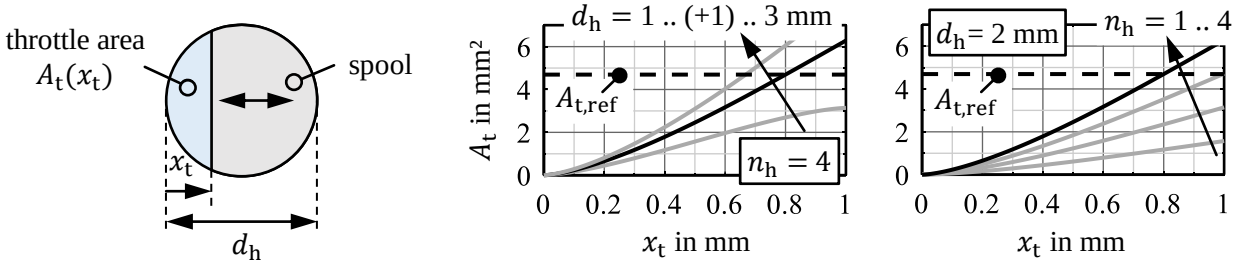

Figure 6: Principal design of spool valve based on cross hole (left), transfer characteristics of spool valve by varying hole diameter and hole number (right)

By moving the spool, the cross section can be enlarged or reduced. The position-dependent opened circular segment is calculated by

$$A_t(x_t) = n_h \left(\frac{d_h^2}{4} \arccos\left(1 - \frac{2x_t}{d_h}\right) - \left(\frac{d_h}{2} - h\right) \sqrt{d_h x_t - x_t^2} \right). \tag{6}$$

With variations of hole diameter d_h and hole number n_h, the behaviour $A_t(x_t)$ can be adjusted to fit the required cross section as shown in **Figure 6** right. The stroke of the full opening should be less than 1 mm, since it is the stable working range of the multi-stable demonstrators, as described above. A suitable combination is $d_h = 2$ mm and $n_h = 4$ with a resulting stroke of 0.8 mm as depicted in **Figure 6** in black. The resulting spool valve design is shown in **Figure 7**.

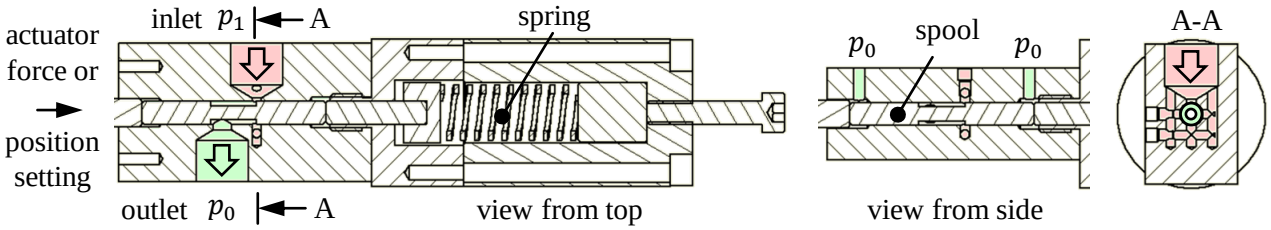

Figure 7: Design of spool valve

The drill holes are the inlet side. Here, tightness between throttle and fitting is possible. The spool is the outlet side. Tightness is here not important due to connection with the ambient pressure p_0. In order to avoid disturbance forces, the spool ends are unloaded with pressure equalisation holes to p_0.

Poppet design

The design of the poppet valve is illustrated in **Figure 8**.

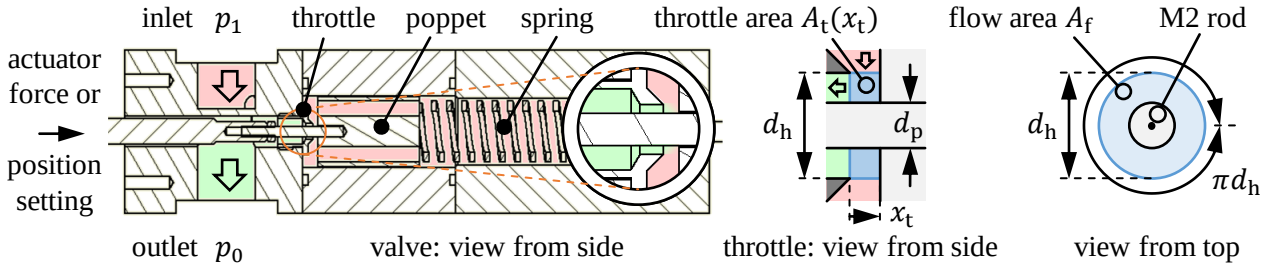

Figure 8: Design of poppet valve (left), principal design of its throttle (right)

The throttle cross section corresponds to the cylindrical surface

$$A_t(x_t) = \pi d_h x_t \tag{7}$$

with the hole diameter d_h according to **Figure 8** middle. The speciality is here the pin through the hole to actuate the poppet by pressing from the left side. It has to be taken into account that the pin reduces the hole area. Thus, it must be ensured that the resulting flow area

$$A_\mathrm{f} = \frac{\pi}{4}\left(d_\mathrm{h}^2 - d_\mathrm{p}^2\right) \tag{8}$$

is greater than the throttle area A_t. By using a M2 rod with a measured diameter $d_\mathrm{p} = 1{,}8$ mm, the hole diameter is set to $d_\mathrm{h} = 3{,}1$ mm resulting in a flow area $A_\mathrm{f} = 5$ mm². By applying eq. (7), the stroke for reaching the reference cross section $A_\mathrm{t,max} = A_\mathrm{t,ref}$ is $x_\mathrm{t,max} \approx 0{,}5$ mm.

4. THROTTLE TRANSFER BEHAVIOUR

Both throttles are investigated concerning its transfer behaviour. First, the real sonic conductance values are determined from measurements to validate the analytical throttle designs. Therefore, the measurement setup according to ISO 6358 in **Figure 9** is used (side view of solenoid test rig in [8]).

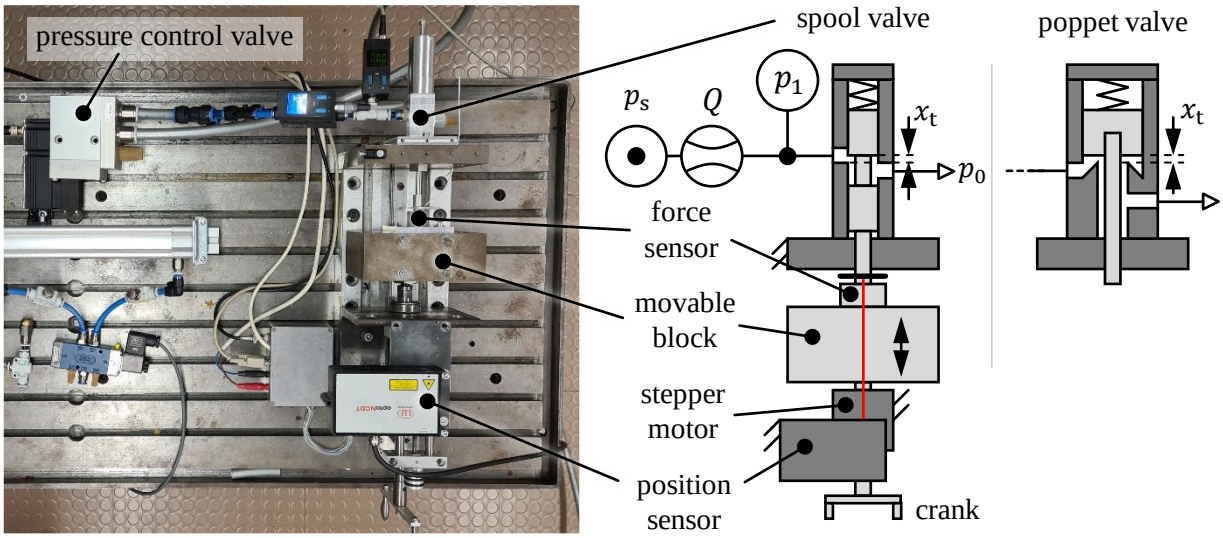

Figure 9: Measurement setup for characterising transfer behaviour of spool and poppet valve

The throttles are opened to the calculated stroke values for $A_\mathrm{t,ref}$ by moving the block to the corresponding position. Then, the pressure difference across the valve is increased and decreased. Therefore, a manual pressure reducing valve is used instead of the installed pressure control valve, shown in **Figure 9**. This is due to control discontinuities of the pressure control valve, especially at low pressures. During the supply pressure variation, the inlet pressure p_1 and volume flow rate Q are measured. **Figure 10** depicts the measurement results $Q(p_1)$ for both valves.

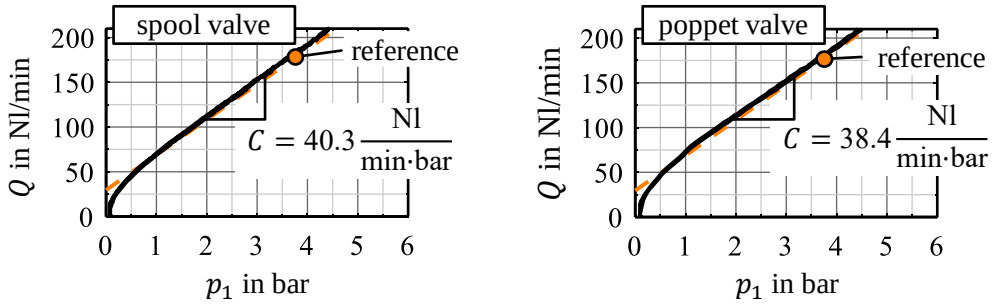

Figure 10: Transfer behaviour $Q(p_1)$ of spool and poppet valve for determining sonic conductance

From the curves, the sonic conductance is evaluated according to eq. (2). The values show a very good match with the reference throttle. Therefore, the designs are validated.

With the same test setup, here with pressure control valve, the transfer characteristic $Q(x, p_s)$ and force behaviour $F(x, p_s)$ are measured. The throttle cross section is increased and decreased by moving the spool and poppet, respectively forward and backward. **Figure 11** shows the resulting behaviour for different supply pressures p_s, which are set by the pressure control valve.

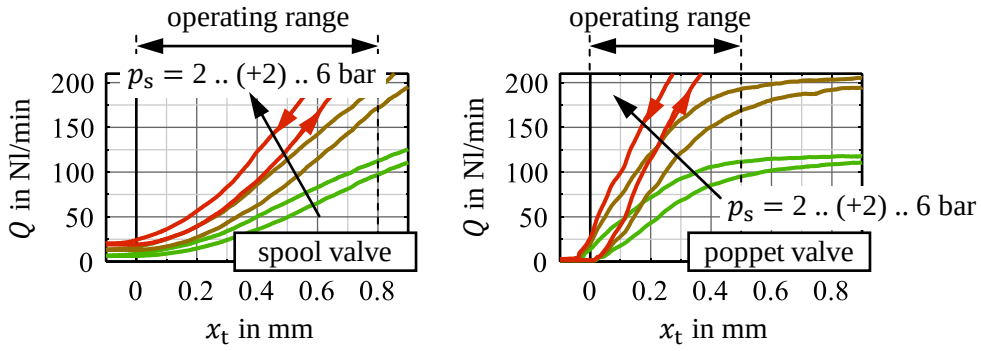

Figure 11: Transfer behaviour $Q(x_t)$ of spool and poppet valve

The curves show principally the expected behaviour. By opening the throttle, the volume flow rate Q increases. At the spool valve, the curves follow the cross section behaviour according to **Figure 6** with its non-linear range at small opening. The behaviour $A_t(x_t)$ of the poppet valve is linear until the flow is dominated by the limiting inner flow area A_f. At the calculated stroke, there is already a throttle effect shown. However, it has no significant influence on the sonic conductance according to **Figure 10**. The real hole diameter is possibly slight larger to compensate the inner throttle effect. Furthermore, the left graph shows at $x_t = 0$ that the spool valve is not tight due to the movement-related gap. This is less a problem in real applications, since the cross section is set to $A_t > 0$ for ensuring cylinder piston movement. The hysteresis effects in the measurements can, for example, be attributed to delays of the flow rate sensor due to its thermal heat-loss measurement principle.

In order to quantify possible disturbances such as friction and pressure force, the measured force behaviour acting to the pin is evaluated. **Figure 12** illustrates the behaviour $F(x_t)$ at the spool valve. It has to be considered that the measurements are done including the spring, whose force can be assumed as constant increasing behaviour.

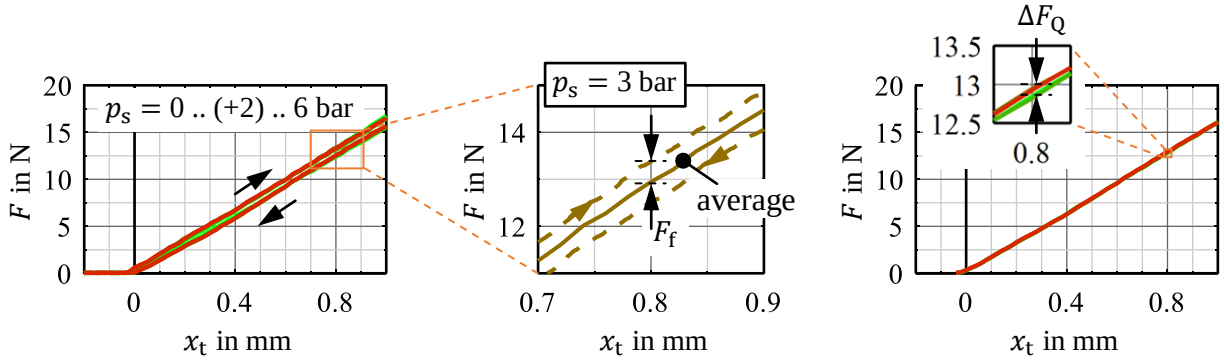

Figure 12: Measured force behaviour at various supply pressures for spool valve

The raw curves at the left side show only small hysteresis, mainly induced by friction forces $F_f \approx 0.4$ N. For investigating the pressure influence, average curves are generated as illustrated in **Figure 12** middle. The comparison of the mean curves at the right side shows only very small flow forces due to different pressures with $\Delta F_Q < 0.15$ N. Thus, the throttle can be assumed as an ideal

load case for the multi-stable solenoid.

The measured force behaviour of the poppet valve is depicted in **Figure 13**.

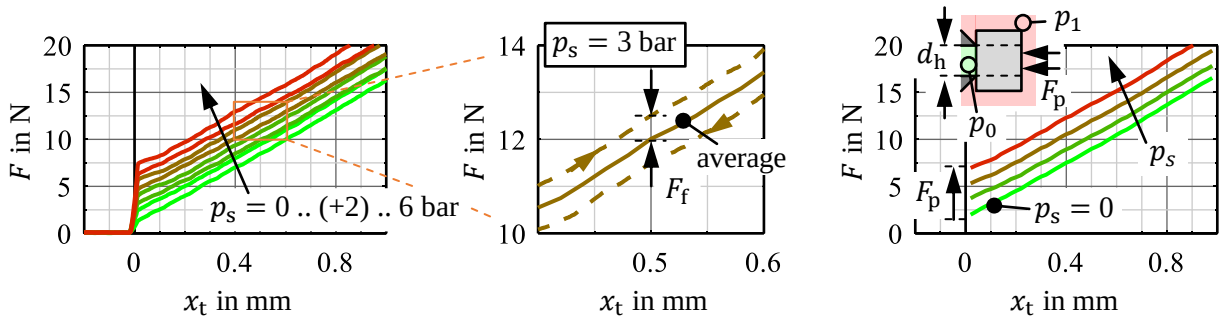

Figure 13: Measured force behaviour at various supply pressures for poppet valve

The hysteresis coming from friction force $F_f \approx 0.5$ N is comparable to the spool valve. The significant difference to the spool valve is the supply pressure dependency. This results from a part area A_p at the poppet's top, which is not pressure-compensated as shown in **Figure 13** right. With increasing pressure, the pressure force

$$F_p = p_1 A_p = p_1 \frac{\pi}{4} d_h^2 \tag{9}$$

increases as well. The theoretical value from the hole diameter $d_h = 3.1$ mm at closing throttle and $p_s = 6$ bar is $F_p = 4.5$ N. The measured value of 5 N differs a bit, possibly caused by the above addressed larger hole area. The pressure force decreases slightly with increasing throttle opening due to different pressure distribution at poppet's bottom.

5. MULTI-STABLE THROTTLE BEHAVIOUR

On the base of the principal transfer characteristics, a multi-stable solenoid is attached to the throttles for demonstrating the setting of any throttle opening and thus any volume flow rate. Firstly, a demonstrator has to be chosen, which roughly matches the force requirement. In order to demonstrate the influence of disturbance forces, the actuator force should be small. The demonstrator with hard ferrite Y35 has the smallest force potential $F_m = 15$ N at $x_a = 2$ mm (see **Figure 3**) and is chosen for the experiments. **Figure 14** illustrates the measured actuator behaviour and the chosen spring characteristic as well as the design of the demonstrator.

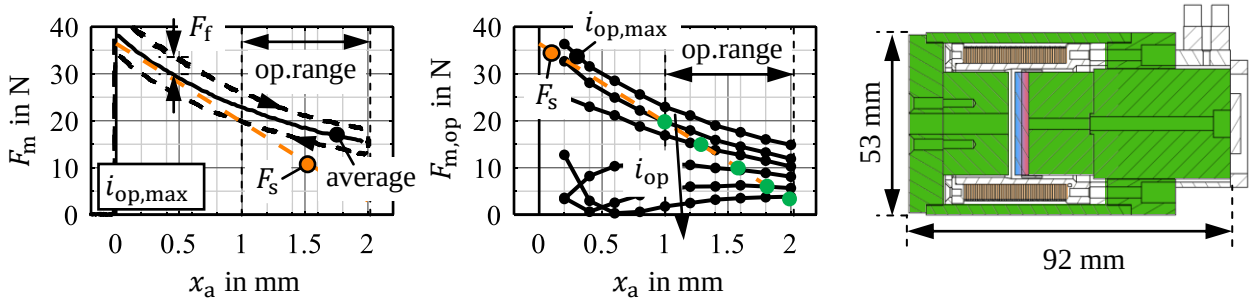

Figure 14: Measured actuator behaviour of the multi-stable demonstrator based on hard ferrite Y35 at full polarisation by moving the armature out and in (left), measured actuator behaviour at fixed positions and variations of polarisation current with remanent operating points at force balance points (middle), half section of used demonstrator (right)

The left side shows a typical force position characteristic with its striking hysteresis, here mainly coming from friction force F_f at the armature. For measuring these curves, the actuator is fully polarised first. Then, the armature is moving out and in, meanwhile the force is measured. This behaviour is utilised to set the spring preload. In addition, **Figure 14** middle shows the remanent magnetic force behaviour at fixed armature. Therefore, the armature is fixed to various positions x_a first. The actuator is then polarised by the current i_op. It results the operating point specific remanent magnetic force $F_\mathrm{m,op}(x_\mathrm{a}, i_\mathrm{op})$, which the figure shows. Depending on the polarisation current, different force curves arise as expected from the actuator principle. In combination with a spring, the remanent armature positions $x_\mathrm{a,op}(i_\mathrm{op})$ result according to the force balance from eq. (1) (green dots).

With this configuration, a working range of approximately 1 mm can be covered. This is sufficient for both, the spool and the poppet valve. It has to be noted that the throttle opening length x_t is inverse to the actuator's air gap (see **Figure 15** right):

$$x_\mathrm{t} = x_0 - x_\mathrm{a}. \tag{10}$$

The throttle is closed approximately at an armature position $x_0 = x_\mathrm{a,max} = 2$ mm.

On that basis, the multi-stable behaviour is investigated. Therefore, the measurement setup seen in **Figure 15** is used. This is based on the measurement setup for throttle characterisation according to **Figure 9**, which is extended by the multi-stable solenoid demonstrator. The actuator is equipped with a position sensor to measure the armature position x_a.

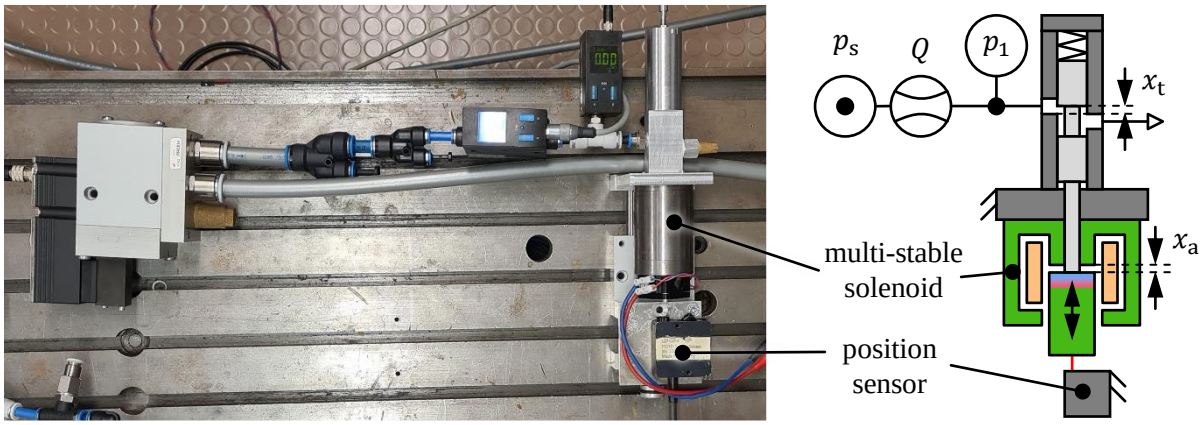

Figure 15: Measurement setup for characterising multi-stable throttle behaviour

With this setup, measurements are done for setting various remanent operating points. Therefore, a polarisation procedure is applied to the solenoid's coil, as exemplary illustrated in **Figure 16** for one operating point (similar to [8]).

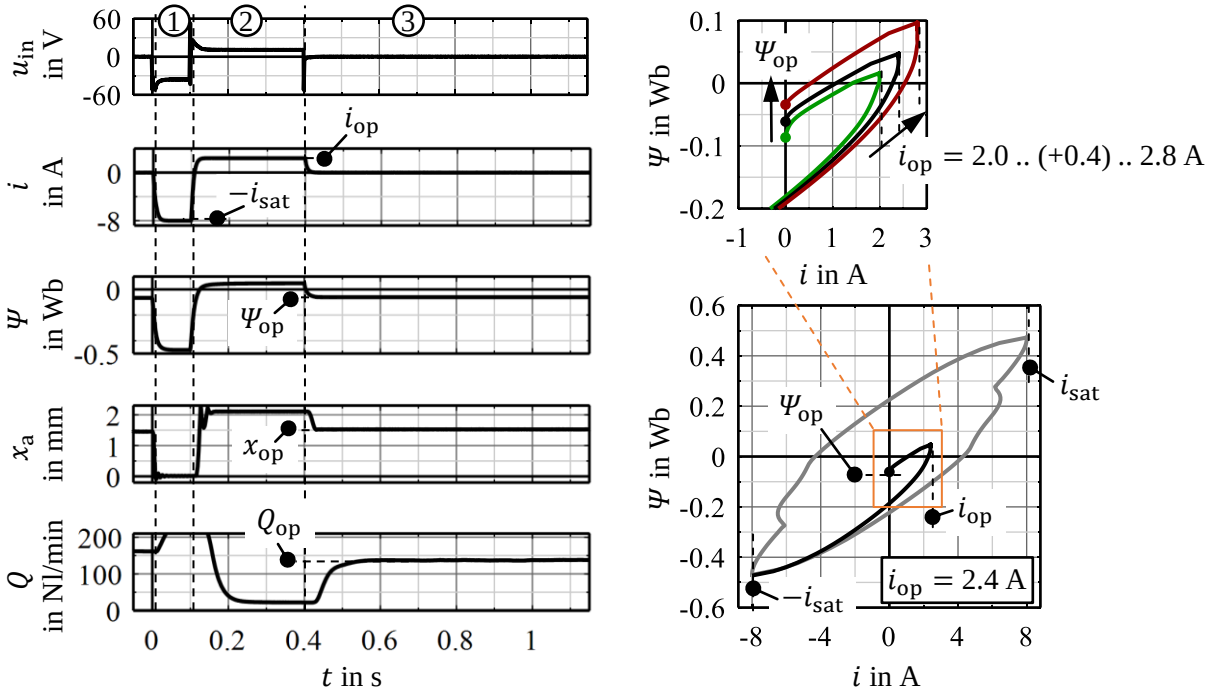

Figure 16: Polarisation procedure for setting the remanent operating point, time-dependent behaviour (left), electro-magnetic behaviour (right)

In the first step, the semi-hard magnetic material is excited to negative saturation, in order to enable a reproduceable reference point. Therefore, the coil current is regulated to $i = -i_{\mathrm{sat}}$. In the second step, the material is polarised to a defined level by regulating the current to i_{op}. At last, the power supply is switched off, the current goes to zero and the remanent operating point sets in. For an inside in the electro-magnetic behaviour, the flux linkage Ψ as summed magnetic flux Φ over all windings w is calculated from input voltage u_{in} and coil current i according to the law of induction with

$$\Psi = w\Phi = \int u_{\mathrm{in}} - Ri \,\mathrm{d}t \tag{11}$$

(see also [8]). **Figure 16** shows at the bottom right side the setting of the remanent flux linkage Ψ_{op} in the electro-magnetic map $\Psi(i)$. The magnetic flux leads directly to a remanent magnetic force, which is simplified yielded according to the Maxwell's pulling force equation

$$F_{\mathrm{m}} = \frac{\Psi_{\mathrm{op}}^2}{2\mu_0 w^2 A_{\mathrm{m}}} \tag{12}$$

with A_{m} as air gap area. In combination with the spring, the armature position x_{a} and thus the throttle position x_{t} is set to a remanent state according to eq. (1) and (10). After the polarisation process, the throttle cross section holds open at the corresponding level without additional power supply. Depending on the inlet pressure p_1 of the throttle, a volume flow rate Q_{op} is established.

By varying the polarisation current i_{op}, the remanent flux linkage Ψ_{op} and thus the remanent magnetic force $F_{\mathrm{m,op}}$ can be set to any level in the operating range as depicted in **Figure 16** top right. Consequently, the volume flow rate Q_{op} can be adjusted as follows. **Figure 17** illustrates the setting of various armature positions $x_{\mathrm{a,op}}$ and volume flow rates Q_{op} depending on the polarisation current i_{op} for the spool valve. Every operating point $(i_{\mathrm{op}}, p_{\mathrm{s}})$ was applied three times to show reproducibility. The shown curves correspond to the average of these three measurements.

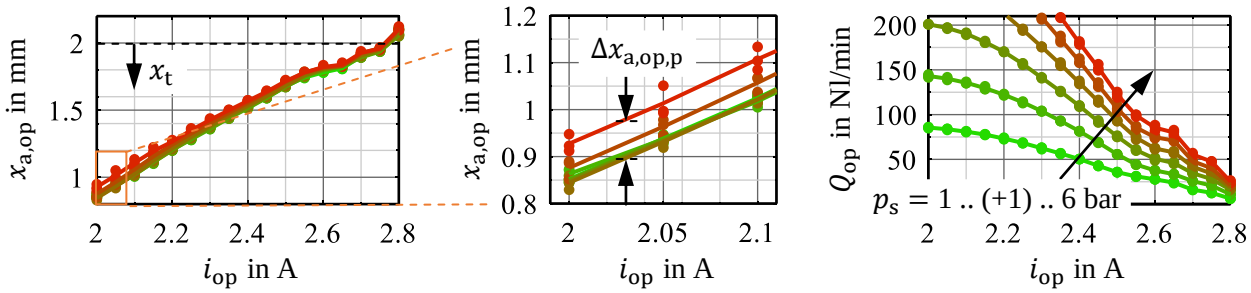

Figure 17: Multi-stable behaviour of armature position (left and middle) and volume flow rate (right) for spool valve

The graphs $x_{a,op}(i_{op})$ and $Q_{op}(i_{op})$ illustrate the basic working principle. Depending on the polarisation current i_{op}, the armature position x_a and thus the volume flow rate Q can be set to any value. The position behaviour is nearly linear as expected from the force balance points in **Figure 14**. Multiple measurements of the same operating point show small deviations up to $\Delta x_{a,op,n} = 0.1$ mm, especially at large throttle opening. Furthermore, the position setting shows a pressure dependency mainly on high pressure levels and large throttle opening, which is in the same size $\Delta x_{a,op,p} \approx 0.1$ mm. Slight flow effects according to **Figure 12**, small deviations in the friction and probably pressure dependent friction conditions in combination with the reduced load stiffness leads to these position deviations. As shown in **Figure 14**, with decreasing armature position, the angle and thus the stiffness between spring and magnetic force curves decrease as well.

In the behaviour of the volume flow rate, deviations can only be slightly seen due to limited measurement range of the sensor. However, it can be noted that the deviations are mainly in the range of large volume flow rates with high supply pressure and large throttle opening. Here are further investigations necessary, for example, with optimised friction behaviour.

The same measurements were done for the poppet valve. The results $x_{a,op}(i_{op})$ and $Q_{op}(i_{op})$ are depicted in **Figure 18**.

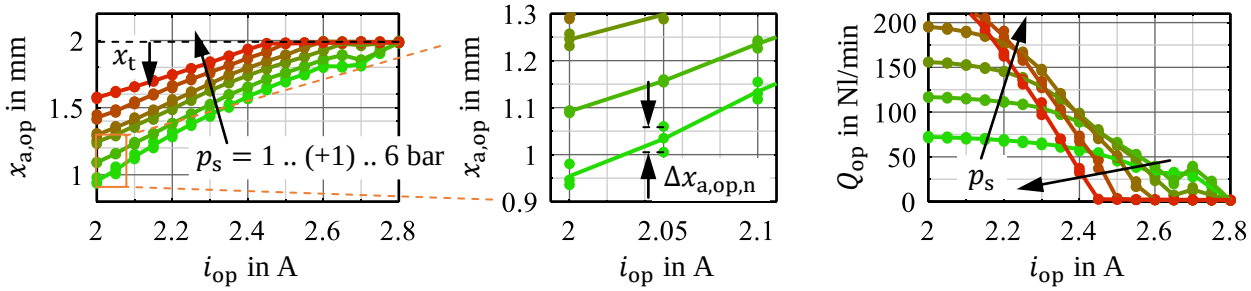

Figure 18: Multi-stable behaviour of armature position (left and middle) and volume flow rate (right) for poppet valve

In the position behaviour, the significant influence of the pressure force can be seen. According to the force balance

$$F_{m,op} = F_s + F_p = F_{s0} - cx_{a,op} + p_1 A_p, \tag{13}$$

the air gap $x_{a,op}$ increases with higher inlet pressure $p_1 \approx p_s$ for an assumed constant magnetic force $F_{m,op}$. This leads to a pressure-dependent throttle cross section and a corresponding influence on the volume flow rate. The effect is inherent for usual poppet valves and can be reduced by designing a valve with a pressure-compensated poppet or by using an actuator with a higher force

potential. With the second, the stiffness against load forces can be increased. Another possibility is the consideration of the pressure dependency in the control law $x_{\mathrm{a,op}}(i_{\mathrm{op}}, \Delta p_{\mathrm{v}})$ by measuring the pressure difference Δp_{v} across the valve during operation.

6. MULTI-STABLE ADJUSTMENT OF CYLINDER PISTON VELOCITY

The throttles with their multi-stable actuator are integrated in a simple pneumatic cylinder drive to demonstrate the adjustability of the piston velocity. The corresponding test setup is illustrated in **Figure 19**.

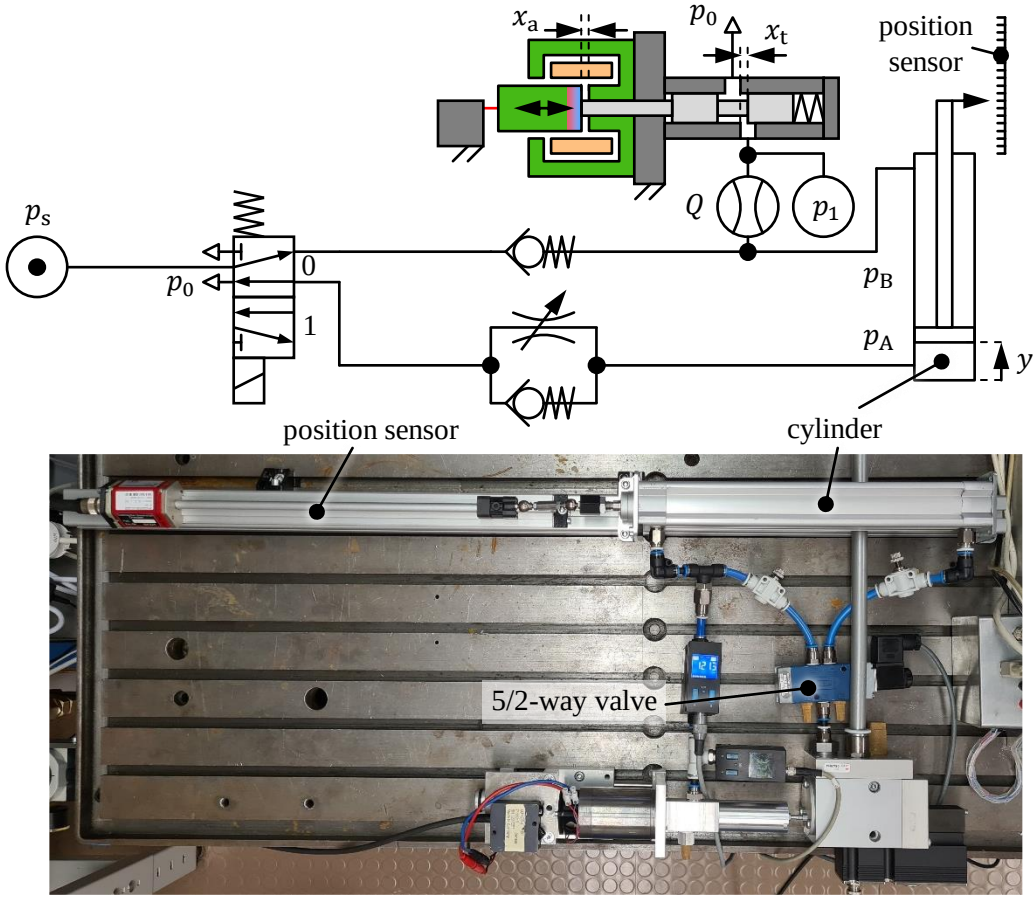

Figure 19: Measurement setup for characterising multi-stable adjustment of cylinder piston velocity

The setup is based on a conventional meter-out control system as shown in **Figure 4**. The throttle check valve for moving out is closed and bypassed by the presented spool or poppet valve. The meter-out has here the advantage of an outlet to ambient. This is important, since the design of the multi-stable solenoid demonstrator is not tight. The cylinder rod is attached to a position sensor. This measures the cylinder piston position y for determining the piston velocity $\dot{y}$. The cylinder has a diameter of 32 mm and a stroke of 250 mm.

With this setup, measurements are done for different supply pressures p_{s} and polarisation currents i_{op}, for every operating point three times. The procedure is as shown in **Figure 20**.

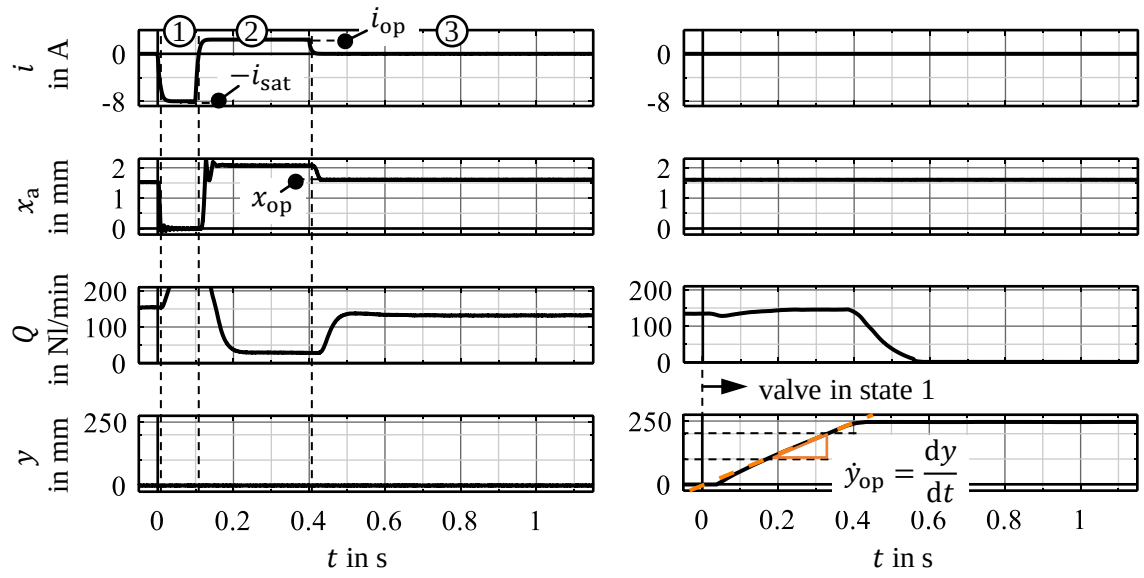

Figure 20: Procedure for setting defined cylinder piston velocity by using the spool valve, polarisation procedure (left), cylinder piston movement (right)

Initially, the 5/2-way valve is in state 0 (move in). The multi-stable solenoid is polarised with the current i_{op} according to the procedure in **Figure 16**. Afterwards, the valve is switched to state 1 for three seconds to move the piston out. At the end, the valve is reset to state 0 for reaching the start condition. During moving out, the velocity is determined by using a regression curve in the range $100\ \mathrm{mm} < y < 200\ \mathrm{mm}$. It is calculated from the derivation

$$\dot{y} = \frac{\mathrm{d}y}{\mathrm{d}t}. \tag{14}$$

The results for the remanent armature position $x_{\mathrm{a,op}}$ and mean piston velocity $\dot{y}_{\mathrm{op}}$ depending on the polarisation current i_{op} by using the spool valve are shown in **Figure 21**.

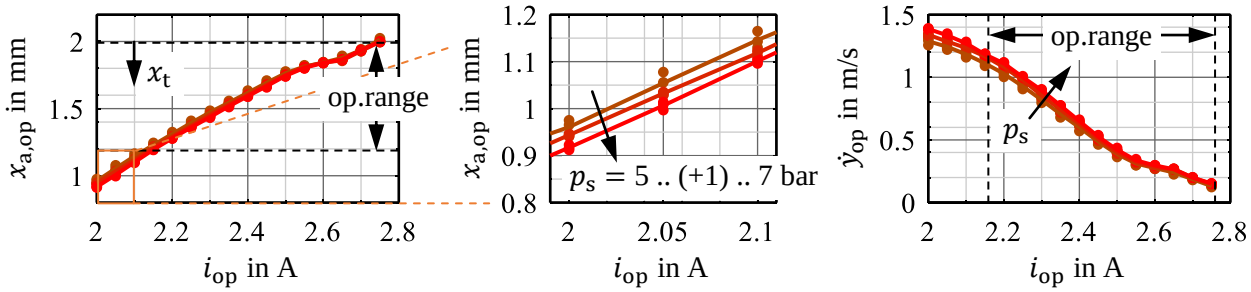

Figure 21: Multi-stable behaviour of armature position (left and middle) and cylinder piston velocity (right) for spool valve

The armature position behaviour is similar to the investigations without cylinder. Here it is noticeable that the pressure dependency of the remanent armature position has the opposite direction in contrast to **Figure 17**. Obviously, the friction conditions has no monotonic dependency from the pressure. This can already be guessed in **Figure 17**. As described above, further investigations are necessary to understand the behaviour in detail for its optimisation.

The resulting piston velocity shows the expected behaviour. Depending on the polarisation current i_{op}, any piston velocity can be set in a nearly linear dependency. The deviations for different supply pressures are slightly higher as expected from the variations of the armature position. This can

be attributed to pressure dynamics after valve switching.

The same measurements were done with the poppet valve. **Figure 22** shows the results.

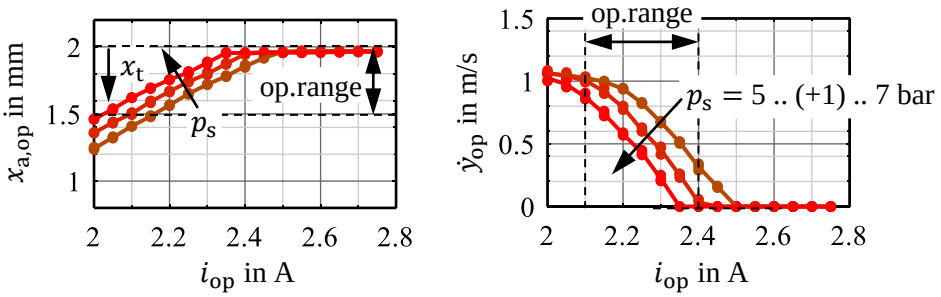

Figure 22: Multi-stable behaviour of armature position (left) and cylinder piston velocity (right) for poppet valve

In principle, the velocity can be set nearly in linear dependence to the polarisation current i_{op} as well. However, the behaviour of the armature position and thus of the piston velocity is influenced by the pressure difference through the valve as described above. Thus, the operating range depends on the pressure and is illustrated in the graphs for $p_s = 6$ bar. As result of the pressure dependency, the armature moves during piston movement as shown in **Figure 23**.

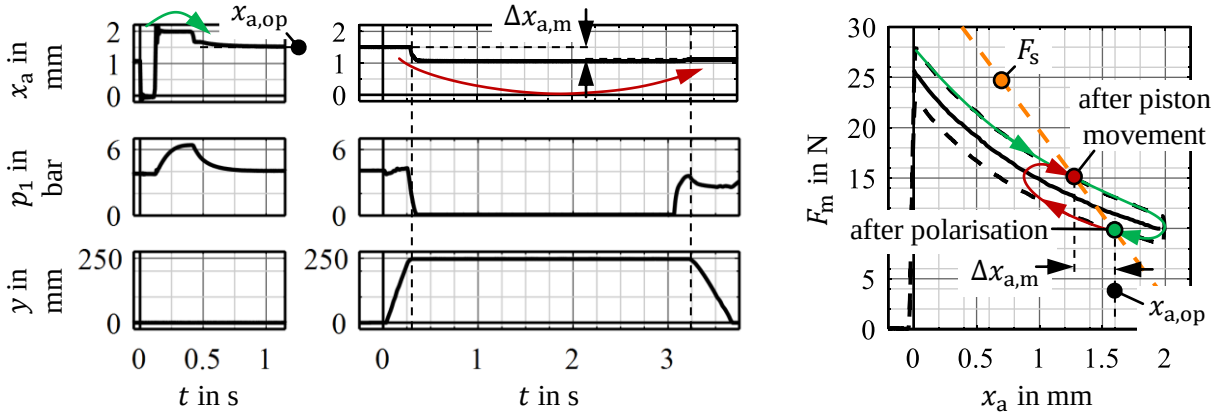

Figure 23: Time-dependent behaviour during polarisation and cylinder piston movement for poppet valve (left), exemplary force behaviour during polarisation and cylinder piston movement (right)

The problem is here a misalignment $\Delta x_{a,m}$ between start and end of piston movement cycle. This comes from armature friction, which depends on the movement direction, as illustrated in the force behaviour in **Figure 23** right. During the polarisation process, the armature comes from above the force balance point $x_{a,op}$ (green line), while it comes after piston movement from below (red line). This is caused by different pressure conditions during piston movement, which acts on the poppet. It results in different remanent armature positions according to armature movement direction due to friction. For solving this issue, the bearing concept has to be improved. For example, friction forces can be reduced nearly to zero by using membrane springs.

The investigations show that multi-stable solenoids are suitable for automating throttle check valves, in order to vary the piston velocity. Therefore, spool valves are preferred due to their very low disturbances. Poppet valves are only usable with additional effort, either by reducing friction and pressure forces or by considering these forces in the control.

7. CONCLUSION AND OUTLOOK

In this work, the automation of pneumatic throttle check valves by using novel multi-stable solenoids is investigated. Based on a conventional throttle check valve, a spool and a poppet valve are designed. Analytical geometrical approaches are used for dimensioning the throttle functionality of the valves. The approaches are validated with measurements. On that basis, the throttles are measured concerning its flow characteristics, which show the expected adjustability by changing the throttle opening section. The spool valve exhibits no significant disturbances and is therefore an ideal load case for multi-stable solenoids. The poppet valve has a significant pressure dependency and is more a real load case for the novel actuator type. The valves are connected to a demonstrator of a multi-stable solenoid, in order to investigate the setting of remanent throttle cross sections. The principal functionality is proven. As expected, the pressure conditions at the poppet valve have an influence on the remanent armature position and thus on the resulting volume flow rate. At the end, the automated throttles are integrated in a pneumatic cylinder drive for demonstrating the setting of different piston velocities. The measurements show that the spool valve in combination with a multi-stable solenoid is well-suited for the automated adjustability of the piston velocity. The poppet valve has too many influences coming from friction and pressure forces and is in this state inappropriate for this task.

Further investigations are dealing with the influence and reduction of friction for optimising the transfer characteristics of the valves. In addition, it is planned to develop a specific multi-stable actuator for the spool valve, which is significantly smaller than the demonstrator used for the investigations here. By using AlNiCo 5 as energy storage material for a force potential $F_{\mathrm{m}} = 18$ N at $x_{\mathrm{a}} = 1$ mm, the actuator volume can be reduced to ca. 30 %. Beside the application of multi-stable solenoids for driving pneumatic throttle check valves, there are a variety of other applications to be investigated. These include, for example, applications in hydraulics or processing technology.

ACKNOWLEDGEMENT

The research presented in this paper is based on the project “Novel multi-stable electro-magneto-mechanical actuators based on variable remanent operating points of semihard- and hard-magnetic materials”, which is funded by the Deutsche Forschungsgemeinschaft (DFG, German Research Foundation) - 434232806.

Funded by

DFG Deutsche Forschungsgemeinschaft

German Research Foundation

NOMENCLATURE

A	area	m^2
B	magnetic flux density	T
d	diameter	m
c	stiffness	N/m
C	sonic conductance	Nl/(min·bar)
F	force	N
H	magnetic field strength	A/m
i	current	A
$\dot{m}$	mass flow rate	kg/s
n	number	-
p	pressure	bar
Q	volume flow rate	Nl/min

R	gas constant	288 (N·m)/(kg·K)
t	time	s
T	absolute temperature	K
u	voltage	V
w	winding number	-
x	position	m
y	piston position	m
$\dot{y}$	piston velocity	m/s
α_d	discharge coefficient	-
μ_0	vacuum permeability	$4\pi \cdot 10^{-7}$ (V·s)/(A·m)
ρ	density	kg/m³
Φ	magnetic flux	Wb
ψ	discharge function	-
Ψ	flux linkage	Wb

REFERENCES

[1] Kallenbach E, Eick R, Ströhla T, et al (2018) Elektromagnete: Grundlagen, Berechnung, Entwurf und Anwendung, 5. Auflage. Springer Fachmedien Wiesbaden, Wiesbaden

[2] Roschke T (2004) Potenzial bipolarer Magnete in Verriegelungs- und Hubanwendungen. In: Innovative Klein- und Mikroantriebstechnik: Vorträge der ETG-/GMM-Fachtagung. Margret Schneider, Darmstadt, Germany

[3] Krauß L (1984) Ein Beitrag zur Auswahl, zum Entwurf und zur Ansteuerung von bipolaren Elektromagneten, insbesondere für Magnetventile. Dissertation, Technische Hochschule Ilmenau

[4] Burmeister LC (1967) NASA Contributions to Advanced Valve Technology - A survey, revised and enlarged edition. National Aeronautics and Space Administration

[5] Johnson BG, Massey SE, Sturman OE (2001) Sturman Digital Latching Valve. Linköping, Schweden, pp 299–314

[6] Olbrich M, Schütz A, Bechtold T, Ament C (2021) Design and Optimal Control of a Multistable, Cooperative Microactuator. Actuators 10:183. https://doi.org/10.3390/act10080183

[7] Uusitalo J-P (2010) A novel digital hydraulic valve package a fast and small multiphysics design. Dissertation, Tampere University of Technology

[8] Kramer T, Weber J (2023) An approach for novel energy-efficient multi-stable solenoids and the demonstration of its fundamental behaviour. In: 18th Scandinavian International Conference on Fluid Power (SICFP 2023). Tampere, Finland

[9] Czichos H, Saito T, Smith LR (2006) Springer handbook of materials measurement methods. Springer, Germany

[10] (2013) ISO 6358-1:2013-05 - Pneumatic fluid power - Determination of flow-rate characteristics of components using compressible fluids - Part 1: General rules and test methods for steady-state flow. ISO

[11] Beater P (2007) Pneumatic drives: system design, modelling and control. Springer, Berlin, London